Article

Investigating the Dielectric Photosensitivity of Zinc Oxide Nanostructures Under Ultraviolet Light

Esmaeil Salahi [1]
https://orcid.org/0000-0002-6673-2058
e.salahi@merc.ac.ir

Hoda Enayati Taloobaghi [2]
https://orcid.org/0009-0001-5016-3532

Mohammad Mahdi Shahidi [3, 4]
https://orcid.org/0000-0001-6389-0547
mmahdishahidi@gmail.com

Fabian I. Ezema [3, 4, 5]
https://orcid.org/0000-0002-4633-1417

Abstract

In this study, we prepared a ZnO thin film using the sol-gel spin-coating method on glass substrates. We repeated the synthesis procedure once, twice and four times to obtain the samples. We then investigated the FESEM images, XRD diffractograms, Hall effect and dielectric measurement of the samples. We observed the phase transition from the wurtzite to the zinc blende phase as a result of the number of repetitions. The films exhibited direct band gaps ranging from 3.2 eV to 3.3 eV. This result indicate that the two-times synthesis process has considerably affected the morphology and also improved the crystallinity of the layer. The sample of which the surface was covered with nearly uniform short nanorod grains with an average diameter of ~ 180 nm showed the highest sensitivity to ultraviolet light.

Keywords: Dielectric properties, photosensitivity, thin film, ZnO

1 Department of Ceramic, Materials and Energy Research Center, Iran.
2 Nano Laboratory, Semnan Science and Technology Park, Iran.
3 Nanosciences African Network iThemba LABS–National Research Foundation, South Africa.
4 UNESCO-UNISA Africa Chair in Nanosciences/Nanotechnology, College of Graduate Studies, University of South Africa.
5 Africa Centre of Excellence for Sustainable Power and Energy Development, University of Nigeria.

UNISA university of south africa PRESS
Nano-Horizons
Volume 3 | 2024 | 12 pages

Nano-Horizons
https://doi.org/10.25159/3005-2602/14260
ISSN 3005-2602 (Online)

Introduction

Ultraviolet detectors based on semiconductors have been widely used in various fields such as optical telecommunications, ultraviolet detection, biological and chemical analysis, and space studies [1]. Generally, silicon-based photodetectors are used to detect light in the ultraviolet range, but since these types of photodiodes are usually sensitive to infrared and visible radiation, they are limited in their optical response in the ultraviolet range. Zinc oxide (ZnO) is one of the transparent semiconductors of group II–VI with a direct and wide band gap. It has a suitable light response in the range of ultraviolet light and is widely used in ultraviolet detectors [2]–[4]. Bulk ZnO with wurtzite crystal structure under ambient conditions is optically uniaxial, meaning that the dielectric function is uniquely defined for the incident light polarised parallel or perpendicular to the optical axis [5]. A higher value of dielectric constant for ZnO nanoparticles can be obtained by doping it with some rare earth metals or transition metals such as Tm and Mn, respectively.

Because ZnO is a non-toxic material, it is safe for humans and the environment and is used in electronic products such as thin film transistors, memory cells and high-speed integrated circuits. Biodegradable polymer nanocomposites based on ZnO can be used as a dielectric material to develop energy storage devices such as capacitors to increase energy density [6].

ZnO is one of the most abundant, biocompatible and non-toxic materials in nature. Because of low-cost and relatively easy manufacturing methods and its good durability against sunlight, ZnO is considered for making optoelectronic devices. At ambient temperature and pressure, ZnO has a wurtzite structure. The structure of ZnO wurtzite has a direct and wide band gap of 3.36 eV at room temperature. When manufacturing optoelectronic components, it is more desirable to use semiconductors that can control and change their energy gap. The excitonic binding energy of ZnO at 300 K is 60 meV. The high binding energy of excitons leads to excitonic recombination and effective excitonic emission at room temperature with low excitation energy [7]–[11].

Electrical properties depend on the quality of the sample. Owing to the difference in the quality of the samples, it is difficult to express the electrical properties of ZnO. The carrier density varies according to the quality of the sample for its type contamination from 10^{16} to 10^{20} electron/cm^2.

Nanoscale ZnO is a very versatile candidate offering diverse applications, for example, gas sensors, piezoelectric transducers, and solar cell windows [12]. In addition, it shows good photoconductivity and high transparency in the visible region because of its wide band gap (3.36 eV) at room temperature and large binding energy (60 meV). The synthesis of oxide nanoparticles with controlled size and shape is crucial in controlling their physical and chemical properties for potential applications in nanotechnology. The effect of the reducing size of oxide nanomaterials can be employed in the commercial

construction and design of solar cells, sensors, catalysts, optics, nanoelectronics and piezoelectric devices.

ZnO nanostructures with high crystalline quality and different morphology can be synthesized through different methods. Various nanostructures such as thin films, spherical nanoparticles, nanowires, nanorods, nanotubes and nanoribbons have been successfully created by methods such as chemical vapour deposition [12], [13], sputtering [14], pulse laser [15], and molecular beam epitaxy [16]. Compared to the mentioned expensive methods, solution-based chemical methods have many advantages such as economic efficiency, low working temperature, and the ability to use different substrates [17], [18]. In this research, we therefore used the spin-coating method, which is a simple chemical method.

Experimental Details

We employed the sol-gel spin-coating technique to prepare a ZnO thin film on a glass substrate, using zinc acetate dihydrate [$Zn(CH_3CO_2)2H_2O$] as the source of zinc. We prepared the precursor solution (0.25 M) by dissolving zinc acetate (99.99%, A.R. Grade, Thomas Baker) in absolute ethanol (99.99%, A.R. Grade, Merck). The mixture was vigorously stirred at 60 °C for 4 hours until a clear and homogeneous solution was obtained.

The solution was deposited onto a pre-cleaned glass substrate by a single wafer spin coater (a homemade instrument). After placing the substrate on the substrate holder of the spin coater, two drops of the coating solution were dispensed and spin coated at 4 000 r/min for 30 seconds in an air atmosphere. The coated substrate was then dried on a hot plate at 50 °C for 60 minutes. This prepared sample was labelled as S1.

The aforementioned procedure was repeated twice and four times to obtain sample S2 and sample S3, respectively. All the prepared samples were annealed at 500 °C for 1 hour in ambient air.

We studied the surface morphology of the samples using a field emission scanning electron microscopy (FESEM). For the structural characterisation of the samples, we used the X-ray diffraction (XRD) D8 Advance Bruker system with Cu-Kα radiation $\lambda = 1.5405$ Å in the 2θ range of 10–80 degrees. To investigate the optical properties, we recorded the absorbance and transmittance spectra of the samples on a UV-Vis Shimadzo-1800 spectrophotometer in the wavelength range of 300–1 100 nm.

Results and Discussion

Morphology Study

FESEM images of prepared ZnO films are shown in Fig. 1. Random orientations of spherical grains with dense structures are observed in sample S1. In sample S2, the surface is covered with short nanorods, approximately uniformly distributed, with an

average diameter of ~180 nm. As observed in this sample, there is a regular structure of grown nanorods that almost completely covers the surface. In sample S3 it is obvious that by increasing the number of synthesis and layering the grains are connected to each other on the surface and there is no opportunity for nanorod growth. This leads to a phase change in the sample and a reduction in crystallite size.

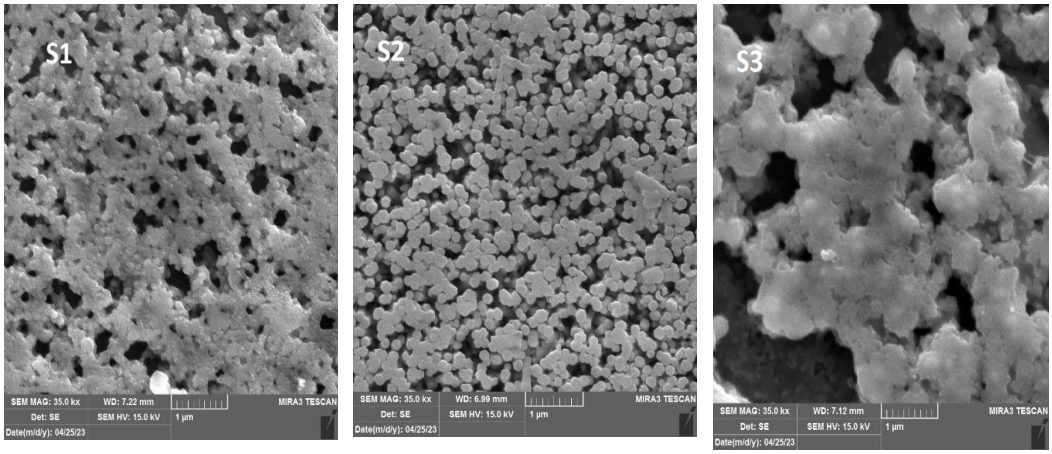

Fig. 1. FESEM images of prepared ZnO films (a) S1, (b) S2, (c) S3.

Structural Properties

Fig. 2 shows the XRD spectra of the studied samples (see also Table I). The data analysis revealed that samples S1 and S2 have a hexagonal polycrystalline structure in the wurtzite phase with (100), (002) and (101) as the preferential directions with little amount of contribution of the zinc blende phase. In sample S3, the wurtzite phase is lost and only the zinc blende phase remains [19], [20]. We conducted an additional analysis of the data of the mean crystallite size, related to the preferential directions, using the Sherrer equation: $D = 0.9\lambda\ \beta\ \cos\theta$, where λ is the full width of half maximum and θ is the Bragg angle. We found it reduces from 8.2 to 8.8 and 8.6 nm in these samples, respectively. The dislocation density (δ) was calculated by [5]: $\delta = 1\ /D^2$.

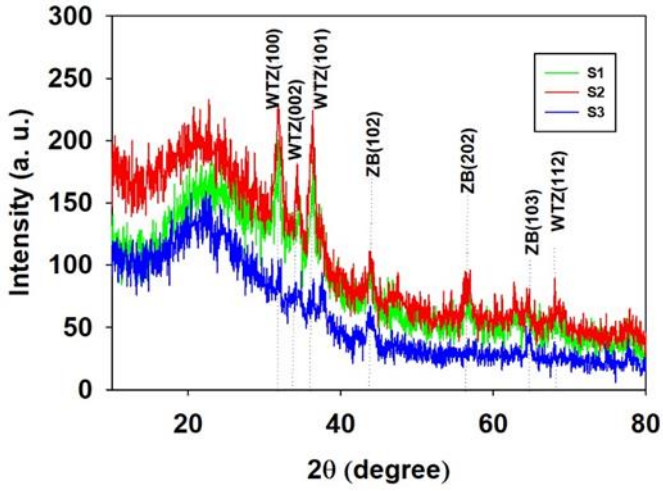

Fig. 2. XRD spectra of the studied samples.

TABLE I
RESULT EXTRACT FROM XRD SPECTRA OF THE STUDIED SAMPLES

No.	**Phase**	***D* (nm)**	***D* (A°)**	**δ (nm^{-2})**
S1	Wurtzite	8.2	2.5	**0.015**
S2	Wurtzite	8.8	2.6	**0.013**
S3	Zinc blende	8.6	2.1	**0.014**

Optical Properties

Fig. 3 shows the transmittance and reflectance spectra of the studied samples. By increasing the number of synthesis times the transparency of the layers is decreased. This could be due to increasing the thickness of the layers, except for sample S2 where the transmittance has increased in the visible area which can be owing to the type of morphology of this sample. Owing to the nanorods structure, the amount of light scattering has decreased. The reflectance of this film shows that in all areas the amount is approximately the same and in sample S2, in the infrared region, the reflectance increased. Also, the absorption spectrum in Fig. 2(c) shows that the second sample has the lowest absorbance in the ultraviolet region. Because of the greater depth of penetration in the ultraviolet region, sample S2 can therefore be a suitable case for optical applications in the ultraviolet or infrared region.

Using transmittance and reflectance spectra and the relation, the direct optical band gap (Eg) of the layers is calculated as shown in Fig. 3(d). To calculate the direct band gap of the samples, we used the equation $(\alpha h\nu)^2 = A(h\nu - Eg)$. In this equation, α represents the absorption coefficient, hν represents the incident radiation energy, and Eg represents the optical band gap. A is a constant. By plotting $(\alpha h\nu)^2$ against hν and extrapolating the linear part of the curve at zero energy, it is possible to determine the band gap. The results show an increasing trend (3.21, 3.28 and 3.30 eV in S1, S2 and S3 samples, respectively). These variations may be related to the crystallinity and phase structure of this layer.

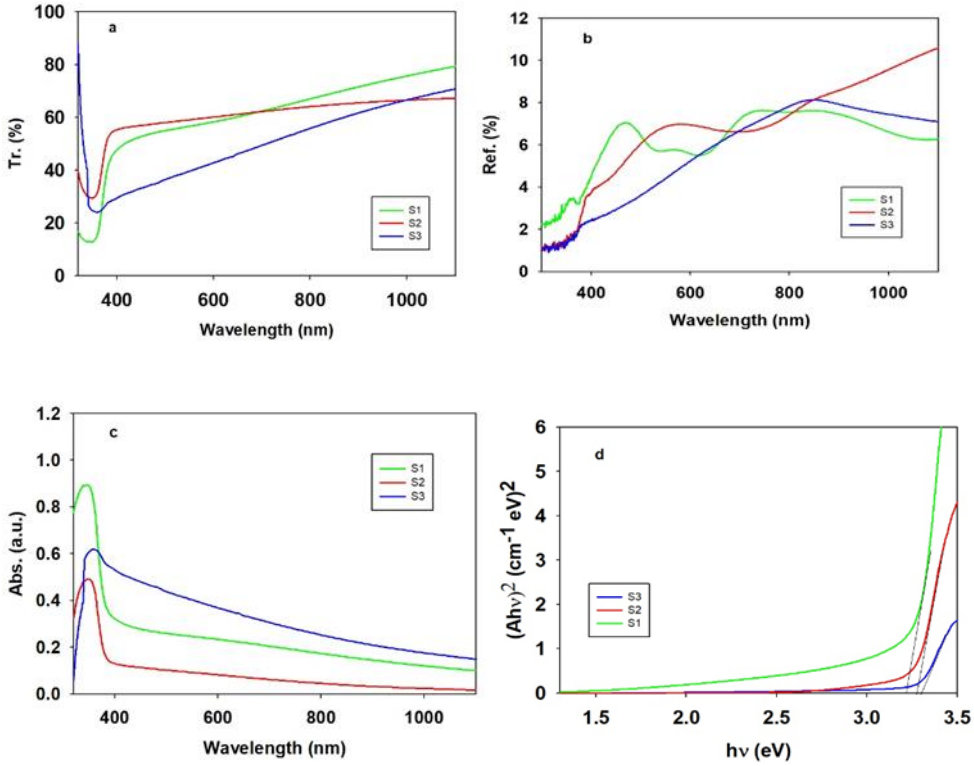

Fig. 3. (a) Transmittance (b) Reflectance (c) Absorption spectra and (d) Energy band gap of the samples.

Electrical Properties

The effects of a number of synthesis on the electrical properties of the samples were evaluated by the Hall effect and resistivity measurements at room temperature (Table II). Fig. 4 illustrates the crystal size, mobility and resistance of the samples for all specimens. As expected, with an increase in the average crystal size, the hole mobility increases, while the electrical resistance of the samples decreases. Meanwhile,

the carrier density has increased from ~ 1.6×10^{17} cm^{-3} in sample S1 to ~ 1.9×10^{18} cm^{-3} in sample S2 and then to ~ 1.7×10^{17} cm^{-3} in sample S3.

Also, we investigated the resistance of the samples in both dark and bright conditions, ie under ultraviolet light. As can be seen, sample S2 shows a higher sensitivity to ultraviolet light. This issue can be related to the nanorod morphology of sample S2. Also, according to the UV spectrum, sample S2 has a lower absorption in the ultraviolet region, which indicates a higher penetration rate of the ultraviolet spectrum in this sample. As a result, ultraviolet light has a greater effect on the properties of sample S2.

TABLE II
DETAIL ANALYSIS ATTRIBUTE HALL EFFECT MEASUREMENT

Sample	**Resistivity (ohm.cm)**	**Carrier density (cm^{-3})**	**Mobility ($cm^2/V.s$)**	**Resistance (kΩ)**	
				dark	**light**
S1	66.8	16×10^{17}	5.84	359.462	359.336
S2	37.5	1.9×10^{18}	8.57	331.429	223.786
S3	43	1.7×10^{17}	8.08	373.400	332.137

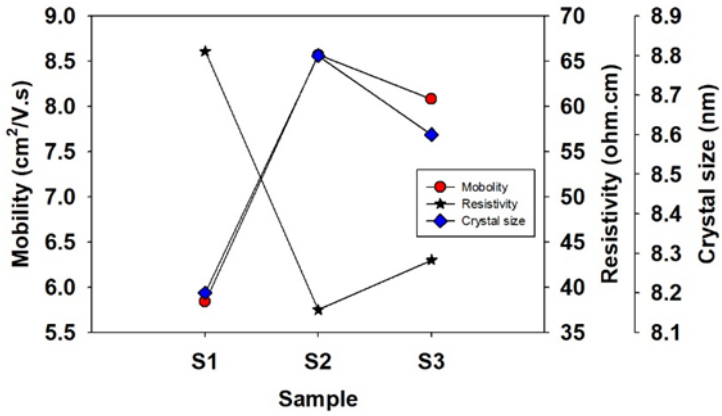

Fig. 4: The variation of resistivity (ρ), hole mobility (μp) , and crystal size (*D*) in the prepared samples.

As can be seen, the mobility is proportional to the changes in the size of the crystals. The increase in the crystal size reduces the scattering of electrons and consequently increases the mobility of the carrier and as a result reduces electrical resistance. As can be seen from Fig. 4, the resistivity has decreased with the increase in crystal size and mobility.

Dielectric Properties

Fig. 5 shows a consistent decrease in dielectric constant (ε) in frequency from 1 kHz to 50 kHz due to the ceasing of polarisations at respective frequency. Owing to the interfacial polarisation available in the nanostructures, the dielectric constant approaches a constant value at a higher frequency region, which is probably due to the rapid polarisation phenomenon in the ZnO material [21].

Fig. 6 shows the dielectric coefficient of the layers which has been measured under dark conditions and under ultraviolet light at different frequencies. As can be seen, the dielectric of all samples decreased at high frequencies and increased at low frequencies. At low frequency, it is known that molecular dipole orientation and ionic conductivity have the greatest effect on dielectric constant. Dipoles created by polarisation mechanisms therefore have enough time to oscillate with frequency. The dielectric constant saturates at high frequency(> 1 MHz) because dipoles are not able to oscillate with frequency. In the prepared samples, the saturation state occurs at a frequency above 40 Hz.

Sample S1 has the highest dielectric value. Surface polarisation with nanograin boundaries improves the dielectric properties, so it is more suitable for capacitor applications. This can be owing to the high resistance of the boundary grains of sample S1, as mentioned in Table II. The Maxwell-Wagner model claims that dielectric materials are materials that consist of grains with high conductivity and low-conductivity grain boundaries are formed [22].

In contrast, sample S2 sample shows the highest sensitivity to ultraviolet light. According to the optical properties of this layer, the high sensitivity can be justified because of to the lower absorption in the ultraviolet region and the higher penetration depth of this sample. The nanorod structure and better crystalline properties of this sample and its higher conductivity can cause higher sensitivity.

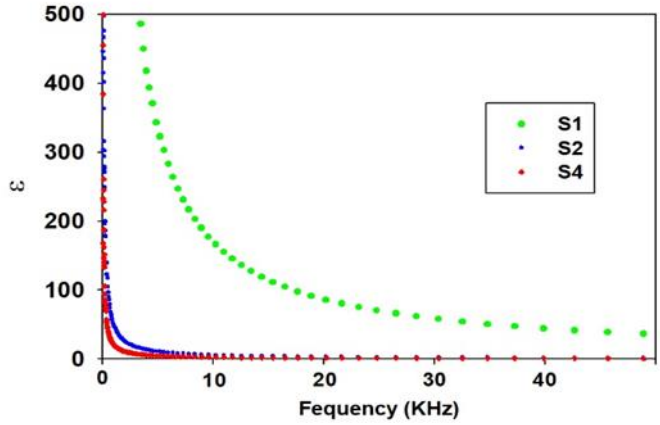

Fig. 6. Dielectric coefficient of the layers.

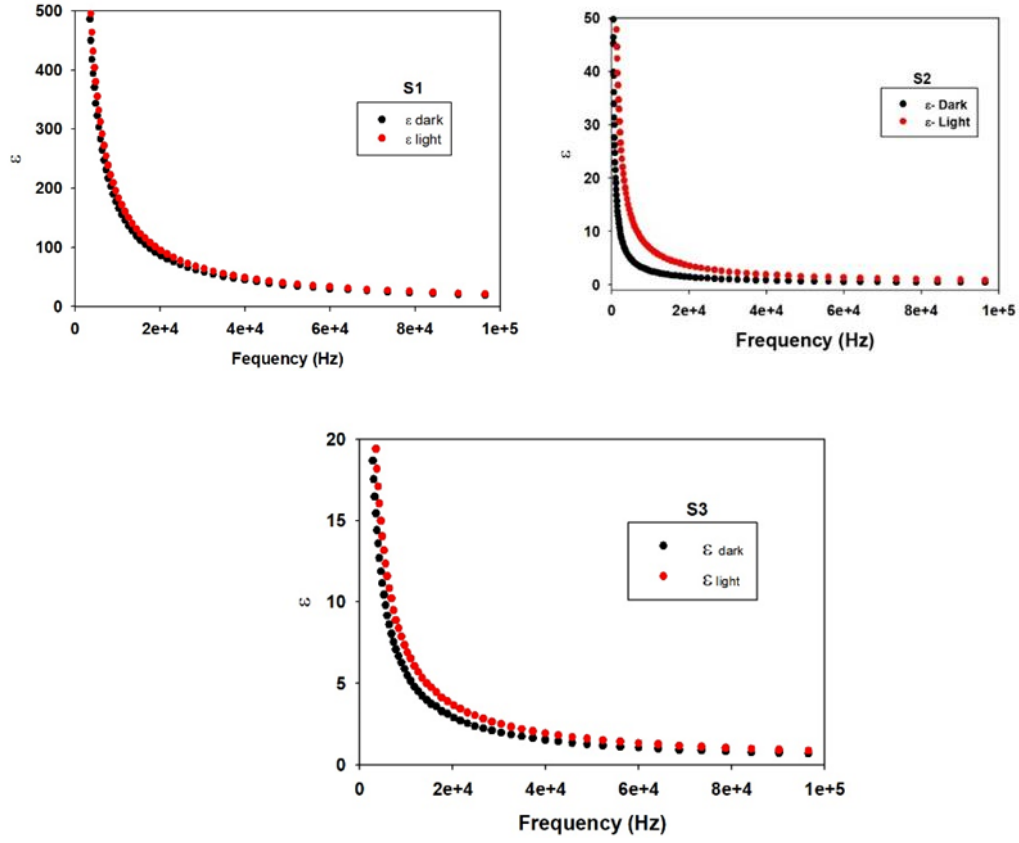

Fig. 5. Dielectric coefficient of the layers in dark and under UV light.

Conclusion

In this research, we investigated the dielectric photosensitivity of ZnO nanostructures under ultraviolet light. The results indicated a phase transition from wurtzite to the zinc blende phase as the number of repetitions increased. The films exhibited direct band gaps ranging from 3.2 eV to 3.3 eV, with the two-times synthesis process significantly affecting the morphology and crystallinity of the layer. The morphological analysis revealed that the surface of the optimally synthesised sample (S2) was covered with short nanorods, leading to a regular structure and high sensitivity to ultraviolet light. X-ray diffraction analysis confirmed the hexagonal polycrystalline structure of the samples. The optical properties of the samples indicated a decrease in transparency with an increase in the number of synthesis times, except for sample S2, which showed increased transmittance in the visible area owing to its unique nanorod morphology.

The reflectance spectra demonstrated consistent reflectance levels in all areas, except for sample S2, which exhibited increased reflectance in the infrared region. Furthermore, sample S2 exhibited the lowest absorbance in the ultraviolet region.

Overall, this study provides valuable insights into the dielectric photosensitivity and optical properties of ZnO nanostructures. The findings contribute to the understanding of the potential applications of ZnO in fields such as ultraviolet detection, optoelectronic devices, and nanotechnology. Further research can explore the practical implementation of ZnO nanostructures in various devices, taking advantage of their unique properties and controllable synthesis methods.

References

[1] E. Monroy, F. Omnès and F. Calle, “Wide-bandgap semiconductor ultraviolet photodetectors,” *Semicond. Sci. Technol.*, vol. 18, no. 4, p. R33, 2003, doi: 10.1088/0268-1242/18/4/201.

[2] P. Capper, S. O. Kasap and A. Willoughby, Zinc Oxide Materials for Electronic and Optoelectronic Device Applications. John Wiley & Sons, 2011.

[3] P. Hazra and S. Jit, “A p-silicon nanowire/n-ZnO thin film heterojunction diode prepared by thermal evaporation,” *J. Semicond.*, vol. 35, no. 1, p. 014001, 2014, doi: 10.1088/1674-4926/35/1/014001.

[4] N. Al-Hardan, A. Jalar, M. A. Hamid, L. K. Keng, N. Ahmed and R. Shamsudin, “A wide-band UV photodiode based on n-ZnO/p-Si heterojunctions,” *Sensor Actuat. A–Phys.*, vol. 207, pp. 61–66, 2014, doi: 10.1016/j.sna.2013.12.024.

[5] A. Djurišić, A. M. C. Ng and X. Chen, “ZnO nanostructures for optoelectronics: Material properties and device applications,” *Prog. Quantum Electron.*, vol. 34, no. 4, pp. 191–259, 2010, doi: 10.1016/j.pquantelec.2010.04.001.

[6] D. Kaur, A. Bharti, T. Sharma and C. Madhu, "Dielectric properties of ZnO-based nanocomposites and their potential applications," *Int. J. Opt.*, vol. 2021, pp. 1–20, 2021, doi: 10.1155/2021/9950202.

[7] C. Jagadish and S. J. Pearton, *Zinc Oxide Bulk, Thin Films and Nanostructures: Processing, Properties, and Applications*. Elsevier, 2011.

[8] J.-J. Dong *et al*., "Controllable synthesis of ZnO nanostructures on the Si substrate by a hydrothermal route," *Nanoscale Res. Lett.*, vol. 8, pp. 1–7, 2013, doi: 10.1186/1556-276X-8-378.

[9] D. Polsongkram *et al*., "Effect of synthesis conditions on the growth of ZnO nanorods via hydrothermal method," *Phys. Rev. B. Condens.*, vol. 403, no. 19–20, pp. 3713–3717, 2008, doi: 10.1016/j.physb.2008.06.020.

[10] C. Pacholski, A. Kornowski and H. Weller, "Self-assembly of ZnO: From nanodots to nanorods," *Angew. Chem. Int. Ed.*, vol. 41, no. 7, pp. 1188–1191, 2002, https://doi.org/10.1002/1521-3773(20020402)41:7%3C1188::AID-ANIE1188%3E3.0.CO;2-5.

[11] A. B. Djurišić and Y. H. Leung, "Optical properties of ZnO nanostructures," *small*, vol. 2, no. 8–9, pp. 944–961, 2006, doi: 10.1002/smll.200600134.

[12] T. D. Steiner, *Semiconductor Nanostructures for Optoelectronic Applications*. Artech House, 2004, doi: 10.1108/sr.2004.24.3.320.3.

[13] T. F. Chung, J. A. Zapien and S.-T. Lee, "Luminescent properties of ZnO nanorod arrays grown on Al: ZnO buffer layer," *J. Phys. Chem. C*, vol. 112, no. 3, pp. 820–824, 2008, doi: 10.1021/jp076618d.

[14] D. Mendil *et al*., "Influence of growth time and substrate type on the microstructure and luminescence properties of ZnO thin films deposited by RF sputtering," *J. Lumin.*, vol. 215, p. 116631, 2019, doi: 10.1016/j.jlumin.2019.116631.

[15] T. Minami, T. Miyata, K. Ihara, Y. Minamino and S. Tsukada, "Effect of ZnO film deposition methods on the photovoltaic properties of ZnO–Cu_2O heterojunction devices," *Thin Solid Films*, vol. 494, no. 1–2, pp. 47–52, 2006, doi: 10.1016/j.tsf.2005.07.167.

[16] A. El-Shaer, A. C. Mofor, A. Bakin, M. Kreye and A. Waag, "High-quality ZnO layers grown by MBE on sapphire," *Superlattices Microstruct.*, vol. 38, no. 4–6, pp. 265–271, 2005, doi: 10.1016/j.spmi.2005.08.025.

[17] N. S. Ridhuan, K. Abdul Razak, Z. Lockman and A. Abdul Aziz, "Structural and morphology of ZnO nanorods synthesized using ZnO seeded growth hydrothermal method and its properties as UV sensing," *PloS One*, vol. 7, no. 11, p. e50405, 2012, doi: 10.1371/journal.pone.0050405.

[18] K. L. Foo, U. Hashim, K. Muhammad and C. H. Voon, "Sol–gel synthesized zinc oxide nanorods and their structural and optical investigation for optoelectronic application," *Nanoscale Res. Lett.*, vol. 9, pp. 1–10, 2014, doi: 10.1186/1556-276X-9-429.

[19] L. E. Greene *et al*., "General route to vertical ZnO nanowire arrays using textured ZnO seeds," Nano Lett., vol. 5, no. 7, pp. 1231–1236, 2005, doi: 10.1021/nl050788p.

[20] S. Aksoy, Y. Caglar, S. Ilican and M. Caglar, "Sol–gel derived Li–Mg co-doped ZnO films: Preparation and characterization via XRD, XPS, FESEM," *J. Alloys Compd.*, vol. 512, no. 1, pp. 171–178, 2012. doi: 10.1016/j.jallcom.2011.09.058.

[21] M. Majeed Khan, R. Siwach, S. Kumar, M. Ahmed and J. Ahmed, "Investigations on microstructure, optical, magnetic, photocatalytic, and dielectric behaviours of pure and Co-doped ZnO NPs," *J. Mater. Sci. Mater. Electron.*, vol. 31, pp. 6360–6371, 2020, doi: 10.1007/s10854-020-03192-2.

[22] M. Bitaraf, M. Ghazi and M. Izadifard, "$CoFe_2O_4$-$BaTiO_3$ nanocomposites; role of ferrite phase on the structural, optical and magnetic properties," *Ferroelectr.*, vol. 613, no. 1, pp. 231–249, 2023, doi: 10.1080/00150193.2023.2215516.